This paper describes objective technical results and analysis. Any subjective views or opinions that might be expressed in the paper do not necessarily represent the views of the U.S. Department of Energy or the United States Government.

SAND2019-10513C

Uncertainty Estimation for Decomposing Carbon Fiber Epoxy Composites

Sarah N. Scott[a*], Victor E. Brunini[b], Andrew J. Kurzawski[c], John C. Hewson[d], Juan P. Hidalgo[e], Rory M. Hadden[f], Stephen Welch[g]

[a]Sandia National Laboratories, Livermore, CA, USA, snscott@sandia.gov

[b]Sandia National Laboratories, Livermore, CA, USA, vebruni@sandia.gov

[c]Sandia National Laboratories, Albuquerque, NM, USA, akurzaw@sandia.gov

[d]Sandia National Laboratories, Albuquerque, NM, USA, jchewso@sandia.gov

[e]School of Civil Engineering, The University of Queensland, St. Lucia, Australia, j.hidalgo@uq.edu.au

[f]School of Engineering, The University of Edinburgh, Edinburgh, UK, r.hadden@ed.ac.uk

[g]School of Engineering, The University of Edinburgh, Edinburgh, UK, s.welch@ed.ac.uk

*Corresponding author

Highlights:

- A computational model of carbon fiber epoxy composites is proposed
- The model is compared to experiments with a range of conditions
- Uncertainty is assessed for model and experiment

Abstract:

Carbon fiber epoxy composites are increasingly used in systems requiring a material that is both strong and light weight, as in airplanes, cars, and pressure vessels. In fire environments, carbon fiber epoxy composites are a fuel source subject to oxidation. This study addresses modeling the thermal response of a carbon fiber composite material through heating and pyrolysis. Using TGA (thermogravimetric analysis) data, a decomposition mechanism is proposed to describe the pyrolysis and smoldering. This is then combined with a finite element conduction-radiation model with a porous media model for gas advection. Mass loss results are compared to cone calorimeter experiments where the composite was exposed to heat fluxes of 30 kW/m^2 and 80 kW/m^2. Two backing materials are compared, aluminum (a heat sink) and ceramic (an insulator). Two thicknesses of the sample are examined, 29 mm and 4.5 mm. A sensitivity study is conducted to understand the uncertainties associated with input parameters, and how these sensitivities change with the heat flux, backing material, and thickness. It is shown that uncertainty increases with increasing heat flux and is higher when a heat sink is used as a backing material compared to an insulation. Contact resistance was found to play a large role in the uncertainty for the thin samples backed with a heat sink.

Keywords: fire, carbon fiber epoxy composite, smoldering, pyrolysis, modeling, uncertainty analysis

Sandia National Laboratories is a multimission laboratory managed and operated by National Technology & Engineering Solutions of Sandia, LLC, a wholly owned subsidiary of Honeywell International Inc., for the U.S. Department of Energy's National Nuclear Security Administration under contract DE-NA0003525.

1. Introduction

Carbon fiber epoxy composites are an attractive engineering material due to their low weight to strength ratio. They have been extensively used in automotive and aeronautical industries, as well as other industries where a light weight, yet strong, material is advantageous. However, unlike more traditional engineering materials like metals, carbon fiber epoxy composites can be a source of fuel in a fire. At temperatures as low as 250°C, epoxies can start to pyrolyze, generating flammable gases. In order to understand the safety risks associated with these materials, it is necessary to understand their behavior when exposed to heating.

Many others have studied the burning behavior of carbon fiber epoxy composites. Quintiere *et al.* explored the behavior of aircraft carbon fiber composites. They found a minimum heat flux for the ignition of the material (18 kW/m^2) and developed a decomposition mechanism for the material [1]. Others have also determined mechanisms for these types of composites as well as thermo-physical properties [2]–[6]. Reviews of the interaction between structural modeling and fire behavior have also been conducted [7]. Higher fidelity models have been created using FireFOAM [8] and FEM codes to understand the implications of the fire on the structure [9].

Recently, Hidalgo *et al.* investigated the behavior of a carbon fiber epoxy composite under a range of thickness and boundary conditions in order to understand the safety risks associated with using these materials in pressure vessels for hydrogen storage [10]–[12].

While experiments investigating the behavior of these materials are invaluable, the range of condtions and scenarios that can be practically tested is constrained by avaiable resources. Validated high fidelity computational models can help fill this gap while also allowing exploration of physical phenomena that cannot be directly measured during experimentation. In addition, they can allow for a range of designs and conditions to be tested to better understand the safety risks. To that end, this paper presents a numerical model for the pyrolysis and smoldering behavior of a carbon fiber epoxy composite. The model uses a porous media plus Arrhenius rate based chemistry modeling technique to describe the decomposition, heat transfer, and flow of pyrolyzate gases of a carbon fiber epoxy composite when exposed to a heat source.

When applied to complex materials such as carbon fiber composites, these models incorporate a high level of complexity due to the number of parameters required. In that sense, validation of such models for complex materials needs to be challenged for a wide range of conditions. In addition to the modeling, this paper compiles the experimental program developed by Hidalgo *et al.*, which explored a range of conditions affecting the heat transfer and reaction rates of a carbon fiber material. Main results are revisited so that assumptions can be incorporated into the numerical pyrolysis and smoldering modeling. The proposed model is compared to a subset of these experimental data for validation purposes. Sensitivity studies are developed to identify the relevance of specific parameters under different conditions from the experiments.

2. Experimental programme setup and main results

The experimental campaign developed by Hidalgo *et al.* consisted of a characterization of the thermal decomposition mechanism at a kinetic regime (TGA), and an extensive bench-scale testing programme using the Cone Calorimeter in two different stages: mass loss measurement and therma penetration measurement. A description of the experimental campaign and discussion of the main results are presented below.

Thermogravimetric studies using isothermal heating of 5 °C/min from ambient temperature up to 850°C showed that, under non-oxidative conditions, the pyrolysis of the epoxy occurred within 300-450°C and a residue of 65-80% of the original mass remained. If tested in air, the thermal decomposition experienced more complex behaviour, with multiple decomposition reaction steps. The reactions occurring within 250 and 400 °C are believed to correspond to different steps of an oxidative pyrolysis process of the epoxy, followed by oxidation of the epoxy residue between 450 and 550 °C. After the epoxy decomposition, the main decomposition reaction responsible of approximately 70% of the mass loss is believed to correspond to the oxidation of the carbon fiber, which occurs between 550 and 810°C. The thermogravimetric results are presented in Fig 6 in combination with the modeling scheme proposed for this work.

The first stage of tests using the Cone Calorimeter aimed at identifying the piloted ignition and burning behaviour. Samples of thickness 4.5 mm and 29 mm (length and width are 100mm) were exposed to heat fluxes within 15-80 kW/m^2. Time-to-ignition, mass loss and combustion product composition measurements were taken. Two bounding backing conditions were used: a 25 mm thick ceramic insulation (insulated condition) and a 25 mm thick aluminum block of 640 g (heat sink). The sides of the samples were wrapped in aluminum foil to restrict the mass transfer through the sides along with a 3 mm thick ceramic insulation paper to reduce the lateral heat losses. Experiments with ceramic insulation were duplicated, whereas experiments with the aluminum heat sink did not include repetitions due to the limited availability of samples in the project.

This first stage allowed identifying distinct thermal behaviours of the composite due to the two backing conditions. As a result, different rates of thermal decomposition could be assessed. Mass loss measurements from all experiments are presented in Fig 1 and Fig 3. Although temperature measurements were not taken for this stage, mass measurements indicate clearly differentiated burning rates for the composite. For the range of heat fluxes studied, the residue left after the end of test was within a range of 60 to 95 %, depending on the heat flux, backing condition and the test duration. This relatively large residue indicates that the predominant reaction was associated with the pyrolysis of epoxy. Two different regimes of mass loss are clearly identified in Fig 1, the first indicative of the pyrolysis of the epoxy and the latter representative of oxidation of the carbon fibers. It can also be identified that at the end of the experiments, samples tested at higher heat fluxes experienced slightly larger mass loss, which can be associated to the oxidation of the carbon fibers at the surface of the samples. This phenomenon was confirmed with visual observations of fibrous ash on the samples top surface, with dense layers of carbon fibers remaining beneath (Fig 2). A conclusion from these tests is that the oxidation of the fibers occurred at a much slower rate than the pyrolysis of the epoxy, which is consistent with the high temperatures required to enable the oxidation reaction. This behaviour is highlighted more clearly in samples tested with a ceramic backing material (adiabatic condition).

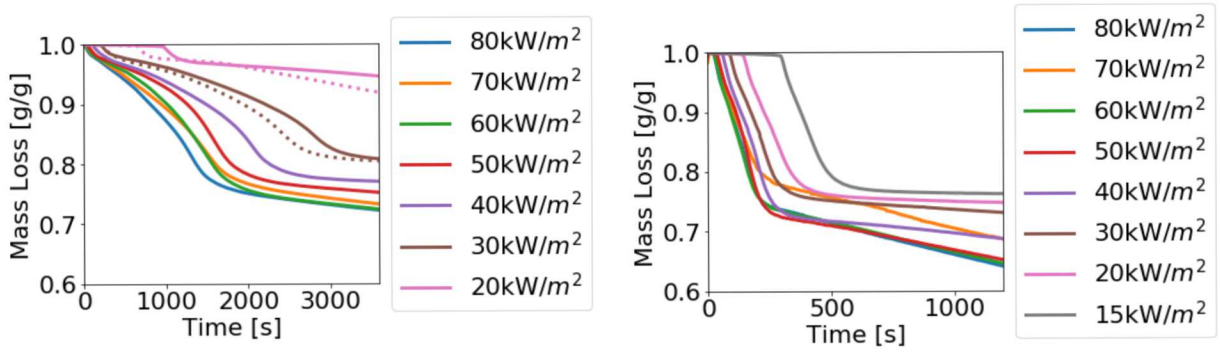

(a) (b)

Fig 1: The mass loss for the ceramic backed samples for the (a) 29 mm sample and (b) the 4.5mm sample. The dotted lines in (a) are repeat experiments.

(a) (b)

Fig 2: 29 mm sample after being tested in the Cone Calorimeter. (a) shows the block of the sample with carbon fibers oxidized on the surface and the rest of the sample being pyrolysed. (b) shows the different layers of carbon fiber detached after pyrolysis.

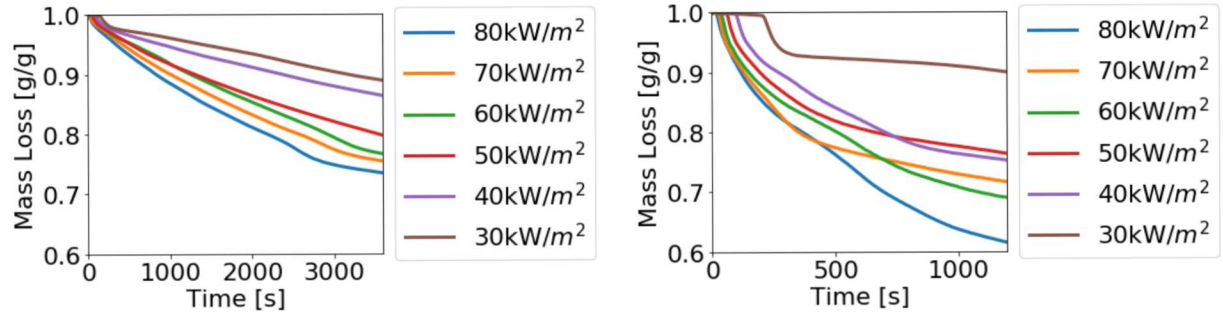

(a) (b)

Fig 3: The mass loss for the aluminum backed samples for the (a) 29 mm sample and (b) the 4.5 mm sample.

In the second stage, samples were further tested under 10 kW/m^2 and 30 kW/m^2, with 1 mm thick Inconel sheathed N-type and 1.5 mm K-ytpe thermocouples inserted in the CFRP at different depths (nominally at 3, 8, 13, 18 and 23 mm from the top surface) and a 1.5 mm thick K-type thermocouple inserted in the aluminum block to allow a better quantification of the back boundary condition. Two experiments were run at 30 kW/m^2 with six thermocouples inserted from the back, and another two with four thermocouples from the side so that the conduction error from the thermocouples would be minimized [14]. Three experiments were run for the for

the 10 kW/m^2 case. The main error included by thermocouple measurements was associated with incorrect positioning of thermocouples, considered as ± 2 mm. Samples were cut after the test and a more precise location of the thermocouple was established and the position corrected. The total mass loss was also measured for these tests.

The second series provided the temperature data that allowed further modeling exercises of varying complexity. The 10 kW/m^2 case represents an case in which there is negligible chemical reaction and the sample behaveas as though inert (confrmed by the low temperature) and the 30 kW/m^2 case represents a case where pyrolysis would be obtained. A pilot was not used so that flaming ignition would not be achieved, thus eliminating the need to quantify the convective and radiative heat flux from the flame.

Temperature measurements from stage 2 are shown in Fig 4. All data from thermocouples is presented, and remeasured thermocouple locations are noted. Repeatability from experiments is shown to be relatively good. Wherever discrepancies are observed, these are attributed to error in the location, as it can be seen that for all experiments the temperature of the aluminum block (29 mm) followed the same temperature evolution. Experiments at 10 kW/m^2 show that the maximum temperature near the surface was below 300 °C, thus confirming that no significant pyrolysis would occur. For 30 kW/m^2, temperatures 2 mm beneath the surface reach maximum values near 500 °C, confirming the composite experienced pyrolysis of the epoxy, oxidation of the char residue from the epoxy pyrolysis, and that carbon fibers did not oxidize.

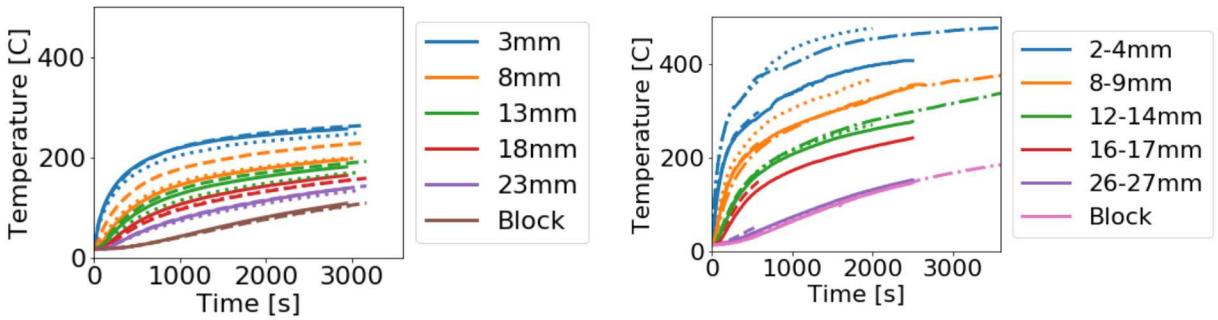

(a) (b)

Fig 4: Temperatures at locations measured from the heated surface for (a) 10 kW/m^2 and (b) 30 kW/m^2. Line style signifies repeat experiments.

3. Computational Model and Uncertainty Quantification Methodology

The pyrolysis and smolder of the carbon fiber is computationally modeled using the Sierra Thermal/Fluids code, Aria, a multiphysics finite element code created at Sandia National Laboratories [14]. The composite is modeled as a porous media, which assumes that there are two phases, the condensed phase and the gas phase. The carbon fiber composite has a certain porosity, which is a function of the decomposition reaction. In the gas phase, Darcy's law is used to approximate the flow of the fluid and the continuity, species, and enthalpy equations are solved. Gases are allowed to enter and exit the domain at specified boundaries. In the continuity equation, density is related to pressure through the ideal gas law so that the gas pressure can be solved. In the condensed phase, the species and enthalpy equations are solved, and the two phases are coupled through source terms in the species equations and a volumetric heat transfer term in the enthalpy equations. This derivation is based on the model by Lautenberger *et al.* [15]

The solid phase continuity equation is:

$$\frac{\partial \rho_b}{\partial t} = -\dot{\omega}'''_{fk} \tag{1}$$

where ρ_b is the bulk density, and $\dot{\omega}'''_{fk}$ is the formation rate of gas phase mass for the k^{th} species from the solid phase. The porous gas phase continuity equation is:

$$\frac{\partial(\bar{\psi}\rho_g)}{\partial t} + \frac{\partial(\rho_g u_{j,g})}{\partial x_j} = \dot{\omega}'''_{fk} \tag{2}$$

where $\bar{\psi}$ is the mixture averaged condensed phase porosity, $\rho_g$is the gas density, and $u_{j,g}$ is the velocity of the gas using the Darcy approximation, which approximates the momentum equation:

$$u_{j,g} = -\frac{\bar{K}}{\mu_g}\left(\frac{\partial p_g}{\partial x_j} + \rho_g g_j\right) \tag{3}$$

where $\bar{K}$ is the mixture averaged solid phase permeability tensor, μ_g is the gas phase viscosity and g_j is the gravity vector. The ideal gas law is used to relate the pressure to the density

$$\rho_g = \frac{\bar{M} p_g}{R T_g} \tag{4}$$

where $\bar{M}$ is the mass averaged molecular weight, R is the gas constant, and T_g is the gas temperature. The final porous gas phase continuity-momentum equation is then:

$$\frac{\partial}{\partial t}\left(\frac{\bar{M} p_g \bar{\psi}}{R T_g}\right) + \frac{\partial}{\partial x_j}\left(\frac{\bar{M} p_g}{R T_g}\frac{\bar{K}}{\mu_g}\left(\frac{\partial \rho_g}{\partial x_j} + \frac{\bar{M} p_g}{R T_g} g_j\right)\right) = \dot{\omega}'''_{fk} \tag{5}$$

The condensed phase species equation is:

$$\frac{\partial(\rho_b Y_k)}{\partial t} = \dot{\omega}'''_{fk} - \dot{\omega}'''_{dk} \tag{6}$$

where $\dot{\omega}'''_{fk} - \dot{\omega}'''_{dk}$ is the difference between the formation and destruction rates of gas phase mass for the k^{th} species and Y_k is the condensed phase mass fraction of the k^{th} species. The gas phase species is:

$$\frac{\partial(\bar{\psi}\rho_g Y_{k,g})}{\partial t} + \frac{\partial(\rho_g u_{j,g} Y_{k,g})}{\partial x_j} = -\frac{\partial q_{k,j}^{Y,g}}{\partial x_j} + \left(\dot{\omega}'''_{s,fk} - \dot{\omega}'''_{s,dk}\right) + \left(\dot{\omega}'''_{g,fk} - \dot{\omega}'''_{g,dk}\right) \tag{7}$$

where $Y_{k,g}$ is the gas phase mass fraction of the k^{th} species, $\left(\dot{\omega}'''_{s,fk} - \dot{\omega}'''_{s,dk}\right)$ is the difference between the formation and destruction rates for solid phase reactions and $\left(\dot{\omega}'''_{g,fk} - \dot{\omega}'''_{g,dk}\right)$ is for gas phase reactions. $q_{k,j}^{Y,g}$ is the gas phase species diffusion flux, defined as:

$$q_{k,j}^{Y,g} = -\bar{\psi}\rho_g D_{k,g} \frac{\partial Y_{k,g}}{\partial x_j} \tag{8}$$

where $D_{k,g}$ is the gas phase mass diffusivity for the k^{th} species. The gas phase enthalpy is:

$$\frac{\partial(\bar{\psi}\rho_g h_g)}{\partial t} + \frac{\partial(\rho_g u_{j,g} h_g)}{\partial x_j} = -\frac{\partial q_{k,j}^{h,g}}{\partial x_j} + \frac{\partial(\bar{\psi} p_g)}{\partial t} + h_{cv}(\bar{T} - T_g) + \sum_k (\dot{\omega}_{s,fk}''' - \dot{\omega}_{s,dk}''') h_{k.g} \tag{9}$$

where h_g is the mixture averaged gas phase enthalpy, h_{cv} is the volumetric heat transfer coefficient, $\bar{T}$ is the porous condensed phase temperature, T_g is the gas phase temperature, $h_{k.g}$ is the gas phase enthalpy of the k^{th} species. $q_j^{h,g}$ is the gas phase energy flux and is modeled as:

$$q_j^{h,g} = -\bar{\psi}\rho_g D_g \frac{\partial h_g}{\partial x_j} \tag{10}$$

where D_g is the mixture averaged gas phase mass diffusivity. The condensed phase enthalpy is defined as:

$$\frac{\partial(\bar{\rho} c_p \bar{T})}{\partial t} = -\frac{\partial q_j^h}{\partial x_j} + h_{cv}(T_g - \bar{T}) \tag{11}$$

where and c_p is the specific heat in the condensed phase and q_j^h is the condensed phase energy flux:

$$q_j^{h,g} = -(k + k_e)\frac{\partial \bar{T}}{\partial x_j} \tag{12}$$

where k is the thermal conductivity and k_e is the effective conductivity for radiant heat transfer in optically thick media.

3.1 Model application

The model was applied to particular conditions defined by the experimental program. The model is first compared to the experimental data where 29 mm thick samples with the aluminium backing material were exposed to a flux of 30 kW/m^2, and temperature and mass loss data were collected. It is then compared to the experimental data were 4.5 mm thick samples with the two backing materials (aluminum and ceramic) were exposed to 30kW/m^2 and 80kW/m^2. As discussed in previous section, only mass loss data was collected for this series. A schematic of both samples is shown in Fig 5.

The domain of the simulation is designed to be a 2D representation of the experiments. For the numerical simulation (for both thicknesses), a structured mesh with an element edge length of 0.45mm was employed. The heat flux was applied on the top surface of the carbon fiber. A

convective boundary condition and a radiative boundary condition were applied to all surfaces. Contact resistance was applied between the sample and the backing material. The values for the boundary conditions are in Table 1.

Parameter	Value / Correlation	Uncertainty	Units
Heat Flux (q)	30	±3%	kW/m^2
Convective Heat Transfer Coefficient (h_{cv})	5	±20%	W/(m^{2}K)
Contact Resistance (R_c)	$0.0003e^{0.0034T}$	-90% +900%	m^{2}K/W

Table 1: Boundary Conditions. The temperature range for contact resistance is 300K to 1000K

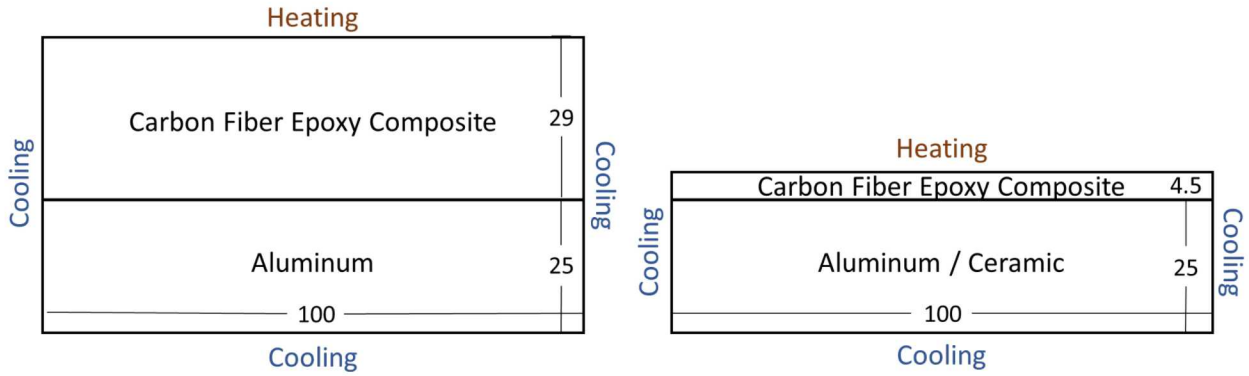

Fig 5: Schematic of the model representing the experiments. Dimensions are in mm.

The material properties used for the backing material are listed in Table 2 [16, 17]. The properties for the carbon fiber epoxy composite are presented in Table 3 [1]. The properties are defined for the constituents of the carbon fiber epoxy composite and are volume averaged to account for the changes in the material properties due to decomposition. Initially, the composition of the compositioe material is 70% carbon fiber, 30% epoxy. All other constituents are 0%. It is assumed that the distribution of the epoxy and carbon fiber is uniform throughout the sample. As the total density of the sampled was measured as 1360 kg/m^3, the initial density of the epoxy is 408 kg/m^3 and the carbon fiber 952 kg/m^3. The difference between these densities and those listed in Table 3 are due to the density here being per total volume of the composite (*e.g.* the mass of the carbon fiber over the volume of the composite), whereas those in the table are per the singular material volume (*e.g.* the mass of the carbon fiber over the volume of the carbon fiber).

Parameter	Value / Correlation		Uncertainty	Units
	Aluminum	***Ceramic***		
Conductivity (k)	$-.0004\,T^2 + 0.4711T + 52.8$	0.7	±10%	W/(mK)
Density (ρ)	2700	1200	±10%	kg/m^3
Specific Heat (c_p)	$0.5039\,T + 745.72$	800	±10%	J/(kgK)
Emissivity (ϵ)	0.1	0.5	±10%	-

Table 2: Nominal material properties and uncertainty for backing material. The temperature range for the aluminum conductivity is 300K to 854K, for aluminum specific heat it is 200K to 600K.

Parameter	Value / Correlation	Uncertainty	Units
Conductivity (k)			W/(mK)
Epoxy	0.145	±35%	
Carbon Fiber	$0.335\ln(T) - 1.8257$	±35%	
Char	0.029	±70%	
Residue	0.00725	±70%	
Density (ρ)			kg/m^3
Epoxy	408	±20%	
Carbon Fiber	952	±20%	
Char	650	±20%	
Residue	2000	±20%	
Specific Heat (c_p)			J/(kgK)
Epoxy	866	±20%	
Carbon Fiber	$4.0997\ T - 369.12$	±20%	
Char	936	±20%	
Residue	866	±20%	
Permeability (K)			m^2
Epoxy	2.42e-15	-90% +900%	
Carbon Fiber	2.42e-14	-90% +900%	
Char	2.83e-12	-90% +900%	
Residue	2.42e-11	-90% +900%	
Radiative Conductivity (k_e)	$16/(3 * 5000)\sigma T^3$	-60% +400%	W/(mK)
Emissivity (ϵ)	0.91	-10% + 8%	-
Initial Carbon Fiber ($\%CF$)	70	±10%	%

Table 3: Nominal material properties and uncertainty for the composite. The simulation properties are defined as the constituents of the carbon fiber epoxy composite and are volume averaged. The temperature range for the carbon fiber conductivity and specific heat for the simulation is 300K to 2328K.

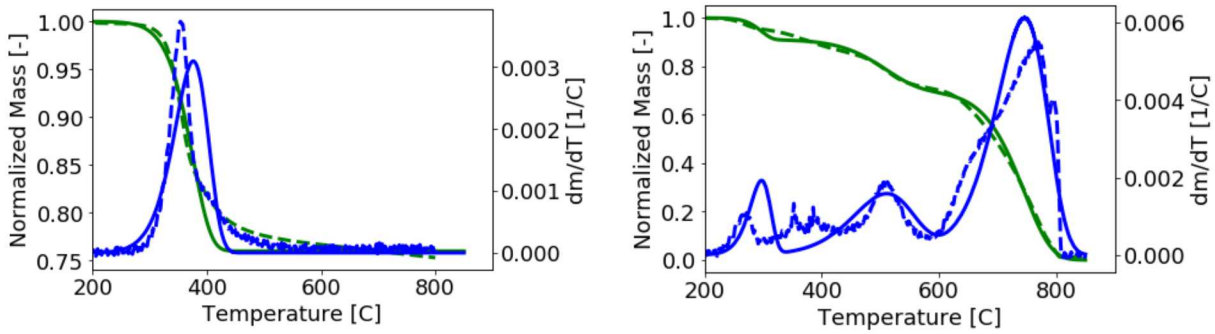

Fig 6: Comparison of the mechanism (solid) to TGA (dashed) [12] for normalized mass loss (green) and the derivative of normalized mass loss (blue) for (a) N_2 purge gas and (b) air purge gas. Note the different scale of the y-axis for (a) and (b).

The TGA results lead to the defining of a chemical mechanism shown in equation 13. As discussed in the experimental section, the epoxy decomposition reaction is likely a non-oxidative

reaction, due to the charring behavior of the composite restricting the flow of oxygen deeper in the composite, and thus should be modeled using results from TGA with a nitrogen purge, rather than in air. For this mechanism, the reaction kinetics for (1a) will be determined using TGA with a nitrogen purge, and the kinetics for (1b), (2), and (3) using TGA with an air purge. The comparison to TGA at 5 °C/min is shown in Fig 6. To apply this mechanism to the model, reaction (1a) is used for the epoxy decomposition, and (1b) is discarded. This merged mechanism is shown in Fig 7.

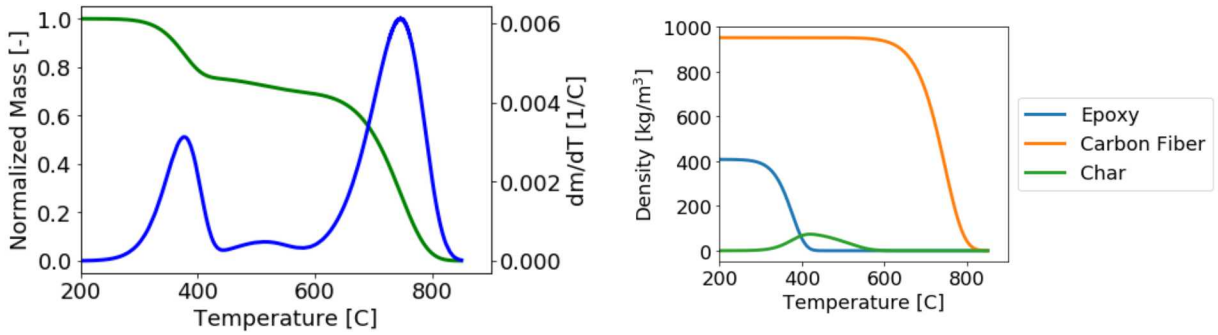

(a) (b)

Fig 7: (a) Comparison of the combined mechanism for normalized mass loss (green) and the derivative of normalized mass loss (blue). (b) Depletion of solid-phase species for combined decomposition mechanism

$$
\begin{aligned}
&\text{(1a)} && Epoxy \rightarrow Char + fuel \\
&\text{(1b)} && Epoxy + O_2 \rightarrow Char + fuel \\
&\text{(2)} && Char + O_2 \rightarrow Residue + gas \\
&\text{(3)} && Carbon\ Fiber + O_2 \rightarrow Residue + gas
\end{aligned}
\qquad (13)
$$

	A		**E_a**		**ν**		**H**	
	[1/s]		*[J/kmol]*		[-]		*[kJ/kg]*	
Reaction 1a	3.33 e6	±10%	1.13 e8	±0%	0.2	±20%	0	±10 [kJ/kg]
Reaction 1b	1.33 e11	-	1.47 e8	-	0.7	-	0	-
Reaction 2	1895	±10%	9.15 e7	±0%	.0001	±0%	12730	±20%
Reaction 3	9.48 e6	±10%	1.90 e8	±0%	.0001	±0%	24770	±20%

Table 4: Kinetic parameters. A is pre-exponential factor, E_a is the activation energy, ν is the stoichiometric coefficient of the solid-phase product (on a mass basis), and H is the heat release.

Model uncertainty and sensitivity are evaluated with Dakota [18] using a Latin Hypercube Sampling (LHS) approach. This method requires a distribution of the input parameters; a uniform distribution is assumed. The range for the uncertainty is tabulated for the property in Table 1 through Table 4. 270 simulations exploring this parameter space were run for each of the configurations. When the LHS method is used, correlation coefficients can be calculated. The Pearson correlation was used to calculate the sensitivity of the input parameter to the output response [19]. Of note, the specific heat and density are varied as one term, ρc_p the volumetric heat capacity, since the uncertainty is a multiplier, and these terms appear together. In addition,

this term is varied for the entire composite, rather than each constituent material to prevent mismatches between products and reactants.

Assessing the experimental uncertainty was more difficult, as due to a limited number of samples, repeat experiments were not always possible. For the mass loss data for the 29 mm thick sample, four repeat experiments were performed. In this case, quantifying the uncertainty was straight forward, as a standard deviation can be calculated from this data. However, for the 4.5 mm thick samples, there were no repeat experiments. Therefore, the data obtained in the 29 mm thick experiments was used to manufacture a possible uncertainty. To do this, first the variance (σ_{total}^2) was calculated for the 29 mm thick data set. Then it was assumed that the variance is made up of the uncertainty associated with the instrument ($\sigma_{instrument}$) in combination with the uncertainty associated with other aspects of the test ($\sigma_{repeatability}$).

$$\sigma_{total}^2 = \sigma_{instrument}^2 + \sigma_{repeatability}^2 \tag{14}$$

Since the σ_{total}^2 and $\sigma_{instrument}$ are known, $\sigma_{repeatability}$ can be solved for. In order to apply this to the 4.5mm thick samples, it was necessary to know what $\sigma_{repeatability}$ was as a function of mass loss. Therefore, the uncertainty at each time (t) was normalized by the data set averaged mass loss ($ML_{average}$) at that time. This quantity was then averaged over time.

$$\sigma_{repeatablity,avg} = \left(\sum_{t=0}^{t=n} \frac{\sqrt{\sigma_{repeatabily,t}^2}}{ML_{average,t}} \right) \Big/ n \tag{15}$$

This yielded an uncertainty of 0.073 per lost gram of material. When combined back with the instrument uncertainty (0.02g), it gives an overall uncertainty of 7.6%, which can now be used as a manufactured uncertainty for the 4.5mm thick results.

A similar issue existed for the thermocouples. While repeat experiments were performed, the thermocouples were not in the same location in the four repeats. In addition, the largest driver of uncertainty here was the location of the thermocouple. It was assumed that the uncertainty could be represented as:

$$\sigma_{total}^2 = \sigma_{instrument}^2 + \sigma_{location}^2 \tag{16}$$

The technique used to drill the holes was accurate within ±2mm. In order to determine the uncertainty in location, the temperature ± 2 mm from the location of interest was interpolated, or if there was a thermocouple in that location, it was given. Assuming a Gaussian distribution of likely thermocouple locations, the temperature uncertainty due to location was calculated. This was then combined with the instrument uncertainty (0.75%) to create an overall temperature uncertainty.

4. Modeling results

Fig. 8 shows the temperature and mass loss prediction along with the experimental results for the 29 mm, 30kW/m^2, aluminum backed sample. The predictions are presented as the average of the 270 runs (the solid line), as well as the range of the predictions (the shaded area). The

uncertainty in the temperature prediction is largest for the middle of the sample, (13 and 17mm), which is also the location of poor agreement between the predictions and the experiment. The mass loss is over-predicted; however, the shape of the mass loss curve matches well with the experiment. Table 5 lists the top three input parameters to which each output response is most sensitive. The temperatures are sensitive to the material properties of the composite, specifically the volumetric heat capacity, the conductivity, the effective conductivity, and the emissivity. As expected, deeper in the composite, the emissivity matters less, and the conductivities matter more. The large uncertainties and poor predictions for the middle of the sample indicates that better models for the volumetric heat capacity and the conductivities are needed. For the mass loss, the initial percentage of carbon fiber is most important, followed by the composite material properties. Since the initial percentage of carbon fiber governs the mass of both the carbon fiber and epoxy, it directly affects the mass loss, since at temperatures below 500°C, only the epoxy has reacted.

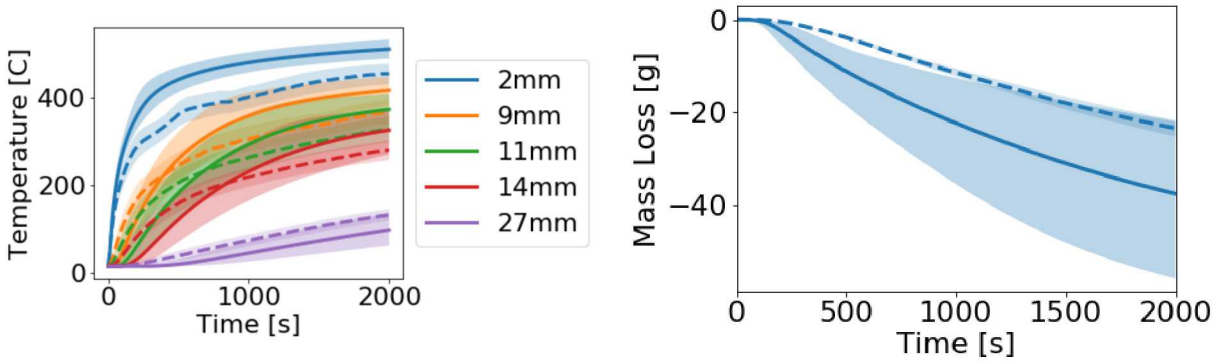

(a) (b)

Fig 8: Comparison of (a) temperature prediction (solid) to experiment (dashed) [11] for six locations measured from the heated surface and (b) the predicted (solid) and experimental (dashed) mass loss for the 29mm, 30kW/m^2, aluminum backed sample. Predictions are presented with min/max bounds and experimental results with one standard deviation of uncertainty.

For the thick sample at a low heat flux, the properties of the aluminum and the contact between the sample and the backing material are of minimal importance. However, this is not so for the thinner samples. Fig 9 shows the temperature and mass loss predictions for the aluminum backing material at 30 kW/m^2 and 80 kW/m^2 flux, while Fig 10 shows the same information for the ceramic. Temperature data was not measured experimentally, therefore only experimental mass loss data is presented. The mass loss predictions are not as good as in the thicker sample because gas-phase ignition occurred but is not modeled. There is qualitative agreement, particularly for the ceramic sample at the higher flux. The mass loss and temperatures between the two holder materials differ because one is a heat sink, and the other is an insulator. The temperatures at 1 mm and 4 mm are spread further apart in the aluminum than in the ceramic – the sample acts thermally thin in the ceramic case, and thermally thick in the aluminum case. The mass loss change reflects this. The sample heats up more uniformly, causing the higher initial mass loss. The plateau in the ceramic backed samples is caused when the epoxy has finished burning off, but the carbon fiber reaction has not yet initiated. In the aluminum backed sample, the epoxy is pyrolyzing for most of the simulation.

2mm	9mm	11mm	14mm	27mm	Mass Loss
Composite ρc_p	Composite ρc_p	Composite ρc_p	Composite ρc_p	Carbon fiber k	$\%CF$
Composite ϵ	Carbon fiber k	Carbon fiber k	Carbon fiber k	Composite ρc_p	Composite ρc_p
$\%CF$	Composite ϵ	Composite ϵ	Composite k_e	Epoxy k	Carbon fiber k

Table 5: Top three sensitive input parameters for each output for the 29mm, 30kW/m^2, aluminum backed sample.

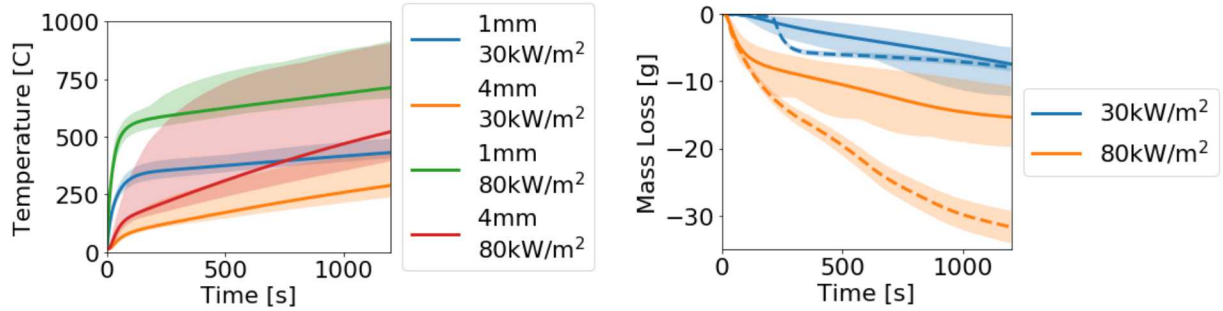

(a) (b)

Fig 9: For the 4.5mm sample at 30kW/m^2 and 80kW/m^2 flux with the aluminum backing material (a) temperature prediction for two locations measured from the heated surface and (b) the predicted (solid) and experimental (dashed) mass loss [12]. Predictions are presented with min/max bounds.

Table 6 lists the top three input parameters that each output response is most sensitive to, for all heat fluxes and backing materials. For the mass loss, the important parameters remain similar for all the heat fluxes and backing material. In all cases, most important is the initial percentage of carbon fiber. The contact resistance, the stoichiometric coefficient of the char in reaction 1a, and the conductivity of the carbon fiber are also important. For the mass loss, the range of the uncertainty bands is not significantly different between the backing materials and the heat fluxes. However, this is not the case with the temperature. Not only does the uncertainty range increase with the flux, but the range is greater in the aluminum backed than in the ceramic backed samples. For example, in the higher heat flux at 4mm, the range at 1200 seconds is 296°C for the ceramic, but 511°C for the aluminum. In addition, the average temperature for the aluminum is near the lower bound, rather than in the middle of the range as it is for the ceramic. The standard deviations for the ceramic and the aluminum are much closer to each other – 60°C and 79°C, respectively. This suggests outlying simulations in the aluminum case where a much larger temperature than average is predicted. Further examination of the data showed that in the case where the contact resistance was at the upper bound of the range, these outlying simulations were generated. This is also reflected in the sensitivities, where for the aluminum the contact resistance plays a large role, whereas it does not appear for the ceramic. In addition, the volumetric heat capacity of the aluminum is important for the prediction of the temperatures, whereas the ceramic's volumetric heat capacity only appears once. This all points to the interaction between the backing material and the sample being more important when it is a heat sink, opposed to an insulator.

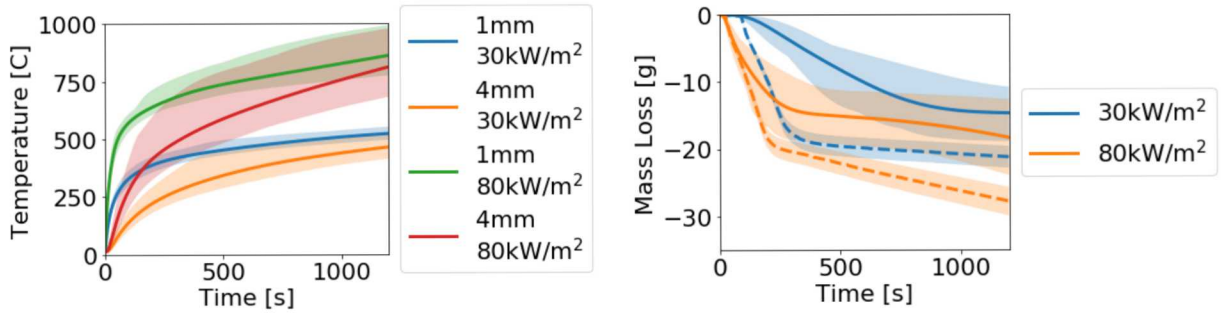

(a) (b)

Fig 10: For the 4.5mm sample at 30kW/m^2 and 80kW/m^2 flux with the ceramic backing material (a) temperature prediction for two locations measured from the heated surface and (b) the predicted (solid) and experimental (dashed) mass loss [12]. Predictions are presented with min/max bounds

	1mm	2mm	3mm	4mm	Mass Loss
Al 30 kW/m^2	Carbon fiber k	R_c	R_c	Carbon fiber k	$\%CF$
	Composite ϵ	Carbon fiber k	Carbon fiber k	R_c	Carbon fiber k
	R_c	Aluminum ρc_p	Aluminum ρc_p	Aluminum ρc_p	R_c
Al 80 kW/m^2	R_c	R_c	R_c	R_c	$\%CF$
	Composite ϵ	Composite ϵ	Carbon fiber k	Carbon fiber k	R_c
	Carbon fiber k	Carbon fiber k	Composite k_e	Aluminum ρc_p	ν
Ceramic 30 kW/m^2	Composite ϵ	Composite ρc_p	Carbon fiber k	Carbon fiber k	$\%CF$
	Composite ρc_p	Carbon fiber k	Composite ρc_p	Composite ρc_p	R_c
	Carbon fiber k	Composite ϵ	Composite ϵ	Ceramic ρc_p	ν
Ceramic 80 kW/m^2	Composite ϵ	Composite ϵ	Carbon fiber k	Carbon fiber k	$\%CF$
	R_c	R_c	R_c	R_c	ν
	Composite ρc_p	Carbon fiber k	Composite ϵ	Composite ϵ	Carbon fiber k

Table 6: Top three input parameters that each output response is most sensitive to for the 4.5mm, samples.

5. Conclusions

An uncertainty estimation and sensitivity study was conducted for a model of decomposing carbon fiber epoxy composite. Five sample configurations were considered:

(1) 29mm thick sample on an aluminum backing material with an external flux of 30kW/m^2

(2) 4.5mm thick sample on an aluminum backing material with an external flux of 30kW/m^2

(3) 4.5mm thick sample on an aluminum backing material with an external flux of 80kW/m^2

(4) 4.5mm thick sample on a ceramic backing material with an external flux of 30kW/m^2

(5) 4.5mm thick sample on a ceramic backing material with an external flux of 80kW/m^2.

Configuration (1) was compared to both temperature and mass loss experimental data. The predictions matched the data well, though the middle of the sample had the worst predictions and most uncertainty. Mass loss was over-predicted, though showed the correct trend. This indicates that changes in the material properties that would better predict the heat transfer properties of the composite, as well as an accurate knowledge of the percentage of epoxy vs carbon fiber in the initial sample would improve the prediction. The temperatures were most sensitive to the properties of the composite, specifically the conductivities and the emissivity. The mass loss was sensitive to the initial ratio of carbon fiber to epoxy, as well as the volumetric heat capacity and the conductivity. For the thinner samples, (2)-(5), uncertainty in the temperature prediction changed with both heat flux and backing material. The aluminum backed samples were more sensitive to the contact resistance than the ceramic. High values of contact resistance created outlying temperature profiles with high temperatures in the aluminum backed cases. The mass loss uncertainty, however, was more uniform across heat fluxes and backing materials.

6. Acknowledgements

The authors would like to acknowledge the valuable contributions of Paulo Pironi to this work. Sandia National Laboratories is a multimission laboratory managed and operated by National Technology and Engineering Solutions of Sandia, LLC., a wholly owned subsidiary of Honeywell International, Inc., for the U.S. Department of Energy National Nuclear Security Administration under contract DE-NA0003525. The reaseach leading to the modeling results has received funding from the Sandia Advanced Simulation and Computing program. The research leading to the experimental results has received funding from the European Union's Seventh Framework Programme (FP7/2007-2013) for the Fuel Cells and Hydrogen Joint Technology Initiative under grant agreement n° 325329.

7. References

[1] J. G. Quintiere, R. N. Walters, and S. Crowley, “Flammability Properties of Aircraft Carbon fiber Structural Composite,” 2007.

[2] A. B. Dodd, B. Shelden, and K. L. Erickson, “Numerical Simulation of Decomposition and Combustion of an Epoxy-Carbon fiber Composite,” in Interflam, 2011.

[3] M. B. McKinnon, Y. Ding, S. I. Stoliarov, S. Crowley, and R. E. Lyon, “Pyrolysis model for a carbon fiber/epoxy structural aerospace composite,” J. Fire Sci., vol. 35, no. 1, pp. 36–61, 2017.

[4] Y. Bai and T. Keller, “Time dependence of material properties of FRP composites in fire,” J. Compos. Mater., vol. 43, no. 21, pp. 2469–2484, 2009.

[5] J. Zhang, M. A. Delichatsios, T. Fateh, M. Suzanne, and S. Ukleja, “Characterization of flammability and fire resistance of carbon fiber reinforced thermoset and thermoplastic composite materials,” J. Loss Prev. Process Ind., vol. 50, pp. 275–282, Nov. 2017.

[6] H. L. N. Mcmanus and G. S. Springer, “High Temperature Thermomechanical Behavior of Carbon-Phenolic and Carbon-Carbon Composites, I. Analysis,” J. Compos. Mater., vol. 26, no. 2, pp. 206–229, 1992.

[7] A. P. Mouritz et al., “Review of fire structural modelling of polymer composites,” Compos. Part A Appl. Sci. Manuf., vol. 40, no. 12, pp. 1800–1814, 2009.

[8] N. Grange, K. Chetehouna, N. Gascoin, A. Coppalle, I. Reynaud, and S. Senave, “One-dimensional pyrolysis of carbon based composite materials using FireFOAM,” Fire Saf. J., vol. 97, pp. 66–75, Apr. 2018.

[9] P. Krysl, W. T. Ramroth, L. K. Stewart, and R. J. Asaro, “Finite element modelling of fiber reinforced polymer sandwich panels exposed to heat,” Int. J. Numer. Methods Eng., vol. 61, no. 1, pp. 49–68, 2004.

[10] J. P. Hidalgo, R. Hadden, S. Welch, and P. Pironi, “Effect of Thickness on the Ignition Behavior of Carbon Fiber Composite Materials used in High Pressure Vessels,” Eighth Int. Semin. Fire Explos. Hazards, pp. 353–363, 2016.

[11] J. P. Hidalgo, P. Pironi, R. M. Hadden, and S. Welch, “A framework for evaluating the thermal behaviour of carbon fiber composite materials,” Eur. Symp. Fire Saf. Sci., pp. 195–200, 2015.

[12] J. P. Hidalgo, R. Hadden, S. Welch, and P. Pironi, “Experimental Study of the Burning Behavior of a Commercial Carbon Fiber Composite Material used in High Pressure Vessels,” in ECCM17 - 17th European Conference of Composite Materials, 2016, p. 8.

[13] P. K. Notz, S. R. Subia, M. M. Hopkins, H. K. Moffat, D. R. Noble, and T. O. Okusanya, “SIERRA Multimechanics Module: Aria User Manual,” Albuquerque, NM, 2016.

[14] J. Beck, “Thermocouple Temperature Disturbances in Low Conductivity Materials,” Journal of Heat Transfer, vol. 84, no. 2, p. 124. 1962

[15] C. Lautenberger and C. Fernandez-Pello, “Generalized pyrolysis model for combustible solids,” Fire Saf. J., vol. 44, no. 6, pp. 819–839, 2009.

[16] American Society for Metals. Metals Handbook Committee, ASM Handbook Volume 2: Properties and Selection: Nonferrous Alloys and Special-Purpose Materials. 1990.

[17] F. Incropera and D. DeWitt, Fundamentals of Heat and Mass Transfer. New York: J. Wiley, 2002.

[18] Dakota Core Team, “Dakota, A Multilevel Parallel Object-Oriented Framework for Design Optimization, Parameter Estimation, Uncertainty Quantification, and Sensitivity Analysis: Version 6.0 Users Manual, SAND2014-4633,” 2014.

[19] S. N. Scott, A. B. Dodd, M. E. Larsen, J. M. Suo-Anttila, and K. L. Erickson, “Validation of Heat Transfer, Thermal Decomposition, and Container Pressurization of Polyurethane Foam Using Mean Value and Latin Hypercube Sampling Approaches,” Fire Technol., vol. 52, no. 1, pp. 121–147, 2016.

Figure captions

Fig 1: The mass loss for the ceramic backed samples for the (a) 29 mm sample and (b) the 4.5mm sample. The dotted lines in (a) are repeat experiments.

Fig 2: 29 mm sample after being tested in the Cone Calorimeter. (a) shows the block of the sample with carbon fibers oxidized on the surface and the rest of the sample being pyrolysed. (b) shows the different layers of carbon fiber detached after pyrolysis.

Fig 3: The mass loss for the aluminum backed samples for the (a) 29 mm sample and (b) the 4.5 mm sample.

Fig 4: Temperatures at locations measured from the heated surface for (a) 10 kW/m^2 and (b) 30 kW/m^2. Line style signifies repeat experiments.

Fig 5: Schematic of the model representing the experiments. Dimensions are in mm.

Fig 6: Comparison of the mechanism (solid) to TGA (dashed) [12] for normalized mass loss (green) and the derivative of normalized mass loss (blue) for (a) N2 purge gas and (b) air purge gas. Note the different scale of the y-axis for (a) and (b).

Fig 7: (a) Comparison of the combined mechanism for normalized mass loss (green) and the derivative of normalized mass loss (blue). (b) Depletion of solid-phase species for combined decomposition mechanism

Fig 8: Comparison of (a) temperature prediction (solid) to experiment (dashed) [11] for six locations measured from the heated surface and (b) the predicted (solid) and experimental (dashed) mass loss for the 29mm, $30kW/m^2$, aluminum backed sample. Predictions are presented with min/max bounds and experimental results with one standard deviation of uncertainty.

Fig 9: For the 4.5mm sample at 30kW/m2 and 80kW/m2 flux with the aluminum backing material (a) temperature prediction for two locations measured from the heated surface and (b) the predicted (solid) and experimental (dashed) mass loss [12]. Predictions are presented with min/max bounds

Fig 10: For the 4.5mm sample at 30kW/m2 and 80kW/m2 flux with the ceramic backing material (a) temperature prediction for two locations measured from the heated surface and (b) the predicted (solid) and experimental (dashed) mass loss [12]. Predictions are presented with min/max bounds

Table 1: Boundary Conditions. The temperature range for contact resistance is 300K to 1000K

Table 2: Nominal material properties and uncertainty for backing material. The temperature range for the aluminum conductivity is 300K to 854K, for aluminum specific heat it is 200K to 600K.

Table 3: Nominal material properties and uncertainty for the composite. The simulation properties are defined as the constituents of the carbon fiber epoxy composite and are volume averaged. The temperature range for the carbon fiber conductivity and specific heat for the simulation is 300K to 2328K.

Table 4: Kinetic parameters. A is pre-exponential factor, Ea is the activation energy, ν is the stoichiometric coefficient of the solid-phase product (on a mass basis), and H is the heat release.

Table 5: Top three sensitive input parameters for each output for the 29mm, 30kW/m^2, aluminum backed sample.

Table 6: Top three input parameters that each output response is most sensitive to for the 4.5mm, samples.